TECHNISCHE MECHANIK, 35, 1, (2015), 31 – 48
submitted: March 15, 2014

In-Plane Stability of Fixed-Fixed Heterogeneous Curved Beams under a Concentrated Radial Load at the Crown Point

L. Kiss, G. Szeidl

The paper by Kiss and Szeidl (2014) is devoted to the stability problem of pinned-pinned shallow curved beams provided that the beam is made of a heterogeneous material and the radius of curvature is constant. The present paper is concerned with the same issue given that the beam is fixed-fixed. Making use of the model presented in Kiss and Szeidl (2014) we aim to (a) determine the critical value of the central load (applied at the crown point) and (b) compare the results with those valid for homogeneous curved beams.

1 Introduction

Though the introduction to paper Kiss and Szeidl (2014) offers a good survey on the preliminaries concerning the investigations planned within the framework of the present paper, it is worth citing here some studies again. The works by Bradford et al. (2002), Pi et al. (2008), Pi and Bradford (2008) present the methodological background as well as the results valid for shallow beams made of homogeneous material. As regards cross-sectional inhomogeneity we should mention the papers Ecsedi and Dluhi (2005), Baksa and Ecsedi (2009) and Kiss (2012), which provide fundamentals for taking this material behaviour into account. The in-plane static and dynamic buckling of shallow pin-ended parabolic arches with a horizontal cable is investigated by Chen and Feng (2010). In paper by Kiss (2014) heterogeneous arches with uniform torsional spring supports are studied using the same kinematical and material assumptions as the present article. Pi and Bradford (2012) deal with the case, when the torsional springs at the ends of the arch have different stiffnesses. In the paper by Silveira et al. (2013) a new numerical strategy is developed for the nonlinear equilibrium and stability analysis of slender curved elements. It is also worth mentioning the model by Bateni and Eslami (2014). In this work the fundamental assumptions are the same as in Bradford et al. (2002), except for one thing: the arch is made of a functionally graded material. In the article by Chen et al. (2014) symmetric pin-jointed kinematically indeterminate structures are investigated. A necessary condition is proposed for the stability of these from the positive definiteness of the quadratic tangent stiffness matrix.

This paper is organized in five Sections and an Appendix. Section 2 is concerned with the fundamental relations and the governing equations for the pre-buckling and post-buckling states. Section 3 provides the formal solutions. Section 4 contains the computational results. The last section is a conclusion in which, a short summary is presented by emphasising the most important results.

2 Pre-buckling State

2.1 Fundamental Relations

Figure 1 shows a fixed-fixed beam, and the applied curvilinear coordinate system, which is attached to the E-weighted centerline (or centerline for short). The former has a constant initial radius ρ_o. The right-handed local base is formed by the unit vectors $\mathbf{e}_\xi$ (tangent to the centerline), $\mathbf{e}_\eta$ (perpendicular to the plane of the centerline) and $\mathbf{e}_\zeta$ (normal to the centerline) – $\mathbf{e}_\eta = \mathbf{e}_\zeta \times \mathbf{e}_\xi$. By cross-sectional inhomogeneity it is meant that the material parameters – the Young's modulus E and the Poisson's number ν – are functions of the cross-sectional coordinates η and ζ (that is, they are independent of ξ): $E(\eta,\zeta) = E(-\eta,\zeta)$, $\nu(\eta,\zeta) = \nu(-\eta,\zeta)$. Otherwise, the material of the beam is isotropic. The cross-section of the curved beam is uniform and symmetric with respect to the

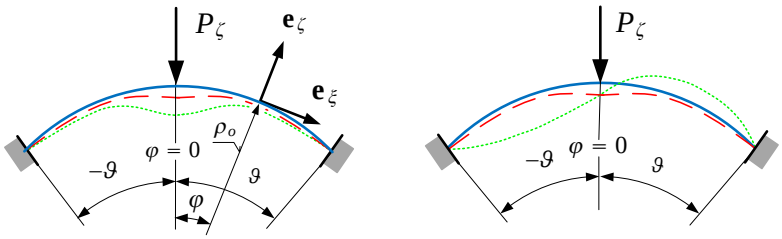

Figure 1: Fixed-fixed beam under a central concentrated load

coordinate plane (ξ, ζ). The centerline, along which the coordinates $\xi = s$ are measured, is assumed to remain in the coordinate plane (ξ, ζ). The position of the point at which the E-weighted centerline intersects the cross-section is obtained from the following condition

$$Q_{e\eta} = \int_A E(\eta, \zeta)\, \zeta \, \mathrm{d}A = 0 \tag{1}$$

in which, the integral is the E-weighted first moment with respect to the axis η – this quantity is denoted by $Q_{e\eta}$. We assume that the displacement vector at an arbitrary point of the cross-section prior to buckling assumes the form

$$\mathbf{u} = \mathbf{u}_o + \psi_{o\eta}\zeta \mathbf{e}_\xi = w_o \mathbf{e}_\zeta + (u_o + \psi_{o\eta}\zeta)\mathbf{e}_\xi \ , \quad \psi_{o\eta} = \frac{u_o}{\rho_o} - \frac{\mathrm{d}w_o}{\mathrm{d}s}, \tag{2}$$

where $\mathbf{u}_o = u_o \mathbf{e}_\xi + w_o \mathbf{e}_\zeta$ is the displacement vector of the centerline, $\psi_{o\eta}$ is the rotation and $s = \rho_o \varphi$ is the arc coordinate. When determining the axial strain ε_ξ we have to use the Green-Lagrange strain tensor. Under the assumption that the nonlinear part of the axial strain ε_ξ is due to the rotation we get the axial strain as

$$\varepsilon_\xi = \frac{1}{1 + \frac{\zeta}{\rho_o}} \left(\varepsilon_{o\xi} + \zeta \kappa_o\right) + \frac{1}{2}\psi_{o\eta}^2, \tag{3}$$

where

$$\varepsilon_{o\xi} = \frac{\mathrm{d}u_o}{\mathrm{d}s} + \frac{w_o}{\rho_o} \ , \qquad \frac{\mathrm{d}\psi_{o\eta}}{\mathrm{d}s} = \kappa_o = \frac{1}{\rho_o}\frac{\mathrm{d}u_o}{\mathrm{d}s} - \frac{\mathrm{d}^2 w_o}{\mathrm{d}s^2} \quad \text{and} \quad \varepsilon_m = \varepsilon_{o\xi} + \frac{1}{2}\psi_{o\eta}^2 \ . \tag{4}$$

Here $\varepsilon_{o\xi}$ and ε_m are the linear and the nonlinear parts of the axial strain on the centerline, while κ_o is the curvature.

We further assume that the elements of the second Piola-Kirchhoff stress tensor satisfy the inequality $\sigma_\xi \gg \sigma_\eta, \sigma_\zeta$. Consequently $\sigma_\xi = E(\eta, \zeta)\varepsilon_\xi$ is Hooke's law. With the knowledge of the stresses we can determine the axial force N and the bending moment M in the pre-buckling configuration

$$N = \int_A E\varepsilon_\xi \, \mathrm{d}A \simeq A_e \varepsilon_m - \frac{I_{e\eta}}{\rho_o}\kappa_o \ , \qquad A_e = \int_A E(\eta, \zeta)\, \mathrm{d}A, \tag{5}$$

$$M = \int_A E\varepsilon_\xi \zeta \, \mathrm{d}A \simeq -I_{e\eta}\left(\frac{\mathrm{d}^2 w_o}{\mathrm{d}s^2} + \frac{w_o}{\rho_o^2}\right) \ , \qquad I_{e\eta} = \int_A E(\eta, \zeta)\zeta^2 \, \mathrm{d}A. \tag{6}$$

In what follows we will make use of the notation

$$m = A_e \rho_o^2 / I_{e\eta} - 1 \approx A_e \rho_o^2 / I_{e\eta} \ . \tag{7}$$

We also change derivatives with respect to s to derivatives with respect to φ by using the following equation

$$\frac{\mathrm{d}^n(\ldots)}{\mathrm{d}s^n} = \frac{1}{\rho_o^n}\frac{\mathrm{d}^n(\ldots)}{\mathrm{d}\varphi^n} = (\ldots)^{(n)} \ ; \quad n \in \mathbb{Z} \ . \tag{8}$$

This transformation is carried out everywhere without a remark. With the knowledge of the bending moment one can check – see Kiss and Szeidl (2014) for details – that

$$N = \frac{I_{e\eta}}{\rho_o^2}\left(\frac{A_e \rho_o^2}{I_{e\eta}} - 1\right)\varepsilon_m - \frac{M}{\rho_o} \approx A_e \varepsilon_m - \frac{M}{\rho_o} \ . \tag{9}$$

2.2 Equilibrium Equations

Assume that the beam is subjected to the distributed forces $\mathbf{f} = f_t\mathbf{e}_\xi + f_n\mathbf{e}_\zeta$, and a central load P_ζ is exerted at the crown point. The central angle of the beam is 2ϑ. For the pre-buckling state, the principle of virtual work can be written as

$$\int_V \sigma_\xi \delta\varepsilon_\xi \,\mathrm{d}V = -P_\zeta \,\delta w_o|_{s=0} + \int_{\mathcal{L}} (f_n\delta w_o + f_t\delta u_o)\,\mathrm{d}s\,. \tag{10}$$

This theorem yields – see Kiss and Szeidl (2014) – the equilibrium equations

$$\frac{\mathrm{d}N}{\mathrm{d}s} + \frac{1}{\rho_o}\left[\frac{\mathrm{d}M}{\mathrm{d}s} - \left(N + \frac{M}{\rho_o}\right)\psi_{o\eta}\right] + f_t = 0 \quad \text{and} \quad \frac{\mathrm{d}}{\mathrm{d}s}\left[\frac{\mathrm{d}M}{\mathrm{d}s} - \left(N + \frac{M}{\rho_o}\right)\psi_{o\eta}\right] - \frac{N}{\rho_o} + f_n = 0\,. \tag{11}$$

Boundary conditions can be imposed on the following quantities

$$N|_{s(\pm\vartheta)} \;\text{ or }\; u_o|_{s(\pm\vartheta)} \qquad | \qquad M|_{s(\pm\vartheta)} \;\text{ or }\; \psi_{o\eta}|_{s(\pm\vartheta)}\,, \tag{12a}$$

$$\left[\frac{\mathrm{d}M}{\mathrm{d}s} - \left(N + \frac{M}{\rho_o}\right)\psi_{o\eta}\right]\Big|_{s(\pm\vartheta)} \;\text{ or }\; w_o|_{s(\pm\vartheta)}\,. \tag{12b}$$

The discontinuity condition

$$\left[\frac{\mathrm{d}M}{\mathrm{d}s} - \left(N + \frac{M}{\rho_o}\right)\psi_{o\eta}\right]\Big|_{s=+0} - \left[\frac{\mathrm{d}M}{\mathrm{d}s} - \left(N + \frac{M}{\rho_o}\right)\psi_{o\eta}\right]\Big|_{s=-0} - P_\zeta = 0 \tag{13}$$

at the crown point should also be satisfied.

2.3 Differential Equations in Terms of Displacements

Upon substitution of equation (9) for the axial force N into $(11)_1$ we get

$$\frac{\mathrm{d}}{\mathrm{d}s}\left(A_e\varepsilon_m\right) - \frac{1}{\rho_o}\left(A_e\varepsilon_m\psi_{o\eta}\right) = 0\,. \tag{14}$$

If, in addition to this, we neglect the quadratic term $\varepsilon_m\psi_{o\eta}$, we arrive at the equation

$$\frac{\mathrm{d}\varepsilon_m}{\mathrm{d}s} \simeq \frac{\mathrm{d}\varepsilon_{o\xi}}{\mathrm{d}s} = 0 \quad \rightarrow \quad \varepsilon_m \simeq \varepsilon_{o\xi} = \text{constant}, \tag{15}$$

which shows, depending on which theory is applied, that the nonlinear/linear strain on the centerline is constant.

If we substitute $\psi_{o\eta}$ from (2), $u_o^{(1)}$ from $(4)_1$ into the expression $\rho_o\varepsilon_m\left(1+\psi_{o\eta}^{(1)}\right)$ and utilize $(4)_3$, we arrive at the following result (the quadratic term is neglected when that is compared to the others)

$$\rho_o\varepsilon_m\left(1+\psi_{o\eta}^{(1)}\right) = \rho_o\varepsilon_m\left[1+\frac{1}{\rho_o}\left(u_o^{(1)} - w_o^{(2)}\right)\right] = \rho_o\varepsilon_m\left[1+\frac{1}{\rho_o}\left(\rho_o\varepsilon_m - w_o - \frac{1}{2}\psi_{o\eta}^2\rho_o - w_o^{(2)}\right)\right] \approx$$

$$\approx \rho_o\varepsilon_m\underbrace{(1+\varepsilon_m)}_{\approx 1} - \varepsilon_m\left(w_o + w_o^{(2)}\right) \approx \rho_o\varepsilon_m - \varepsilon_m\left(w_o^{(2)} + w_o\right)\,. \tag{16}$$

Substitute now formulae (6) and (9) into $(11)_2$ and take equations (15)-(16) into account. After some manipulations we have

$$W_o^{(4)} + \left(\chi^2+1\right)W_o^{(2)} + \chi^2 W_o = \chi^2 - 1\,, \qquad \chi^2 = 1 - m\varepsilon_m\,. \tag{17}$$

Here and in the sequel $W_o = w_o/\rho_o$ and $U_o = u_o/\rho_o$ are dimensionless displacements. Equation (17) can be compared with the equation that Bradford, Pi et al. have used in their series of articles published recently on stability problems of shallow arches – e.g., Bradford et al. (2002); Pi et al. (2008). This equation is of the form

$$W_o^{(4)} + (\chi^2 - 1)W_o^{(2)} = \chi^2 - 1. \tag{18}$$

2.4 Solutions to the Pre-buckling State

The general solution satisfying equation (17) is sought separately on the right ($W_{o\,r}$) and on the left ($W_{o\,\ell}$) half beam (due to the discontinuity in the shear force at the crown point) in the form

$$W_{o\,r} = \frac{\chi^2-1}{\chi^2} + A_1\cos\varphi + A_2\sin\varphi - \frac{A_3}{\chi^2}\cos\chi\varphi - \frac{A_4}{\chi^2}\sin\chi\varphi\,, \tag{19a}$$

$$W_{o\,\ell} = \frac{\chi^2-1}{\chi^2} + B_1\cos\varphi + B_2\sin\varphi - \frac{B_3}{\chi^2}\cos\chi\varphi - \frac{B_4}{\chi^2}\sin\chi\varphi\,. \tag{19b}$$

Here A_i and B_i $(i=1,\ldots,4)$ are undetermined integration constants. These can be determined with the knowledge of the boundary conditions. Let us now introduce the following function

$$H(\varphi) = \begin{cases} -1 & \varphi < 0 \\ 1 & \varphi > 0\,. \end{cases} \tag{20}$$

After determining the constants of integration A_i from the boundary and discontinuity conditions imposed on the

Table 1: Boundary conditions for the fixed-fixed beam

Boundary conditions	
Crown point	Right end
$\psi_{o\eta}\big\vert_{\varphi=+0} = 0$	$W_o\vert_{\varphi=\vartheta} = 0$
$-\frac{\mathrm{d}M}{\mathrm{d}s}\big\vert_{\varphi=+0} + \frac{P_\zeta}{2} = 0$	$\psi_{o\eta}\big\vert_{\varphi=\vartheta} = 0$

Boundary conditions	
Crown point	Right end
$W_{o\,r}^{(1)}\Big\vert_{\varphi=+0} = 0$	$W_{o\,r}\vert_{\varphi=\vartheta} = 0$
$I_{e\eta}W_{o\,r}^{(3)}\Big\vert_{\varphi=+0} = \frac{P_\zeta}{2}$	$W_{o\,r}^{(1)}\Big\vert_{\varphi=\vartheta} = 0$

right half beam (see Table 1) we can unify the two solutions as

$$W_o = \frac{\chi^2-1}{\chi^2} + A_{11}\cos\varphi - \frac{A_{31}}{\chi^2}\cos\chi\varphi + \left(A_{12}\cos\varphi + A_{22}H\sin\varphi - \frac{A_{32}}{\chi^2}\cos\chi\varphi - \frac{A_{42}}{\chi^2}H\sin\chi\varphi\right)\frac{\mathcal{P}}{\vartheta}, \tag{21}$$

where

$$\begin{aligned} A_1 &= \frac{1-\chi^2}{\mathcal{D}\chi}\sin\chi\vartheta + \frac{1}{\mathcal{D}(1-\chi^2)}(\cos\vartheta\,\cos\chi\vartheta + \chi\sin\vartheta\,\sin\chi\vartheta - 1)\frac{\mathcal{P}}{\vartheta} = A_{11} + A_{12}\frac{\mathcal{P}}{\vartheta}\,, \\ A_3 &= \frac{1}{\mathcal{D}}\left(1-\chi^2\right)\sin\vartheta + \frac{\chi}{\mathcal{D}(1-\chi^2)}\left(\chi - \sin\vartheta\,\sin\chi\vartheta - \chi\cos\vartheta\,\cos\chi\vartheta\right)\frac{\mathcal{P}}{\vartheta} = A_{31} + A_{32}\frac{\mathcal{P}}{\vartheta}\,, \\ A_2 &= \frac{1}{\chi^2-1}\frac{\mathcal{P}}{\vartheta} = A_{22}\frac{\mathcal{P}}{\vartheta}\,, \qquad A_4 = \frac{\chi}{\chi^2-1}\frac{\mathcal{P}}{\vartheta} = A_{42}\frac{\mathcal{P}}{\vartheta}\,, \end{aligned} \tag{22a}$$

and

$$\mathcal{D} = \chi\cos\vartheta\,\sin\chi\vartheta - \sin\vartheta\,\cos\chi\vartheta\,. \tag{22b}$$

With these in hand

$$\begin{aligned} \psi_{o\eta} = U_o - W_o^{(1)} \simeq -W_o^{(1)} &= A_{11}\sin\varphi - \frac{A_{31}}{\chi}\sin\chi\varphi + \\ &+ \left(A_{12}\sin\varphi - A_{22}H\cos\varphi - \frac{A_{32}}{\chi}\sin\chi\varphi + \frac{A_{42}}{\chi}H\cos\chi\varphi\right)\frac{\mathcal{P}}{\vartheta} = \\ &= D_{11}\sin\varphi + D_{31}\sin\chi\varphi + (D_{12}\sin\varphi + D_{22}H\cos\varphi + D_{32}\sin\chi\varphi + D_{42}H\cos\chi\varphi)\frac{\mathcal{P}}{\vartheta} \end{aligned} \tag{23a}$$

is the rotation field if we assume that the tangential displacement has a negligible effect. The constants D_{ij} $i\in[1,2,3,4]$; $j\in[1,2]$ are defined by

$$D_{11} = A_{11}\,, \quad D_{12} = A_{12}\,, \quad D_{22} = -A_{22}\,, \quad D_{31} = -\frac{A_{31}}{\chi}\,, \quad D_{32} = -\frac{A_{32}}{\chi}\,, \quad D_{42} = \frac{A_{42}}{\chi}\,. \tag{23b}$$

It follows from the equilibrium equation (15) that the axial strain $(4)_1$ is constant on the centerline. Let us calculate the mathematical average of this quantity

$$\varepsilon_m \;=\; \frac{1}{\vartheta}\int_0^{\vartheta} \varepsilon_m(\varphi)\mathrm{d}\varphi \;=\; \frac{1}{\vartheta}\int_0^{\vartheta} \left(\varepsilon_{o\xi} + \frac{1}{2}\psi_{o\eta}^2\right)\mathrm{d}\varphi \;=\; I_{ow} + I_{1w}\frac{\mathcal{P}}{\vartheta} + I_{o\psi} + I_{1\psi}\frac{\mathcal{P}}{\vartheta} + I_{2\psi}\left(\frac{\mathcal{P}}{\vartheta}\right)^2 \tag{24}$$

or, which is the same

$$I_{2\psi}\left(\frac{\mathcal{P}}{\vartheta}\right)^2 + \left(I_{1w} + I_{1\psi}\right)\frac{\mathcal{P}}{\vartheta} + \left(I_{ow} + I_{o\psi} - \varepsilon_m\right) = 0\,. \tag{25}$$

The integrals $I_{ow}, \ldots, I_{2\psi}$ are all given in a closed form in the Appendix.

3 Post-buckling State

3.1 General Relations

As regards the post-buckling equilibrium state, we remark that quantities denoted by an asterisk belong to the post-buckling equilibrium state while the change (increment) between the pre- and post-buckling equilibrium is denoted by a subscript $_b$. Following this rule of decomposition, for the rotation field and the change of curvature we can write

$$\psi_{o\eta}^* = \psi_{o\eta} + \psi_{o\eta\,b}\,, \quad \psi_{o\eta\,b} = \frac{u_{ob}}{\rho_o} - \frac{\mathrm{d}w_{ob}}{\mathrm{d}s}\,, \quad \kappa_o^* = \kappa_o + \kappa_{o\,b}\,, \quad \kappa_{o\,b} = \frac{1}{\rho_o}\frac{\mathrm{d}u_{ob}}{\mathrm{d}s} - \frac{\mathrm{d}^2 w_{ob}}{\mathrm{d}s^2}\,. \tag{26}$$

As regards the strain increment, on the base of (4), we have

$$\varepsilon_\xi^* = \varepsilon_\xi + \varepsilon_{\xi\,b}\,, \qquad \varepsilon_{\xi\,b} = \frac{1}{1+\frac{\zeta}{\rho_o}}\left(\varepsilon_{o\xi\,b} + \zeta\kappa_{o\,b}\right) + \psi_{o\eta}\psi_{o\eta\,b} + \frac{1}{2}\psi_{o\eta\,b}^2\,, \quad \varepsilon_{o\xi\,b} = \frac{\mathrm{d}u_{ob}}{\mathrm{d}s} + \frac{w_{ob}}{\rho_o}\,, \tag{27}$$

and

$$\varepsilon_{mb} = \varepsilon_{\xi\,b}|_{\zeta=0} = \varepsilon_{o\xi\,b} + \psi_{o\eta}\psi_{o\eta\,b}\,. \tag{28}$$

We remark that the rotational term quadratic in the increment has been neglected since we assume that $\frac{1}{2}\left|\psi_{o\eta\,b}^2\right| \ll |\psi_{o\eta}\psi_{o\eta\,b}|$.

By utilizing equations (5)-(6) for the axial force we can write

$$N^* \;=\; \int_A E\varepsilon_\xi^*\,\mathrm{d}A \;=\; N + N_b\,, \quad \text{where} \quad N_b \;=\; \frac{I_{e\eta}}{\rho_o^2}\left(\frac{A_e\rho_o^2}{I_{e\eta}} - 1\right)\varepsilon_{mb} - \frac{M_b}{\rho_o} \;\approx\; A_e\varepsilon_{mb} - \frac{M_b}{\rho_o}, \tag{29}$$

which coincides formally with equation (9). Due to the presence of the term ε_{mb} this result is nonlinear. It can be checked with ease by recalling (6) that

$$M^* = \int_A E\varepsilon_\xi^*\zeta\,\mathrm{d}A = M + M_b\,, \quad \text{where} \quad M_b = -I_{e\eta}\left(\frac{\mathrm{d}^2 w_{ob}}{\mathrm{d}s^2} + \frac{w_{ob}}{\rho_o^2}\right). \tag{30}$$

With regard to equations (29) and (30) it follows that

$$N_b + \frac{M_b}{\rho_o} = A_e\varepsilon_{mb}\,. \tag{31}$$

3.2 Equilibrium Equations in Terms of Increments

Under the assumption that P_ζ does not change its value or direction (so $P_\zeta^* = P_\zeta$), the principle of virtual work for the buckled equilibrium configuration assumes the form

$$\int_V \sigma_\xi^*\delta\varepsilon_\xi^*\,\mathrm{d}V = -P_\zeta^*\;\delta w_o^*|_{s=0} + \int_{\mathcal{L}}\left(f_n^*\delta w_o^* + f_t^*\delta u_o^*\right)\,\mathrm{d}s\,. \tag{32}$$

After some manipulations, which are detailed in Kiss and Szeidl (2014), it can be shown that the arbitrariness of the virtual quantities yields the equations

$$\frac{\mathrm{d}N_b}{\mathrm{d}s} + \frac{1}{\rho_o}\frac{\mathrm{d}M_b}{\mathrm{d}s} - \frac{1}{\rho_o}\left(N + \frac{M}{\rho_o}\right)\psi_{o\eta\,b} - \frac{1}{\rho_o}\left(N_b + \frac{M_b}{\rho_o}\right)\psi_{o\eta\,b} + f_{tb} = 0\,, \tag{33a}$$

$$\frac{\mathrm{d}^2 M_b}{\mathrm{d}s^2} - \frac{N_b}{\rho_o} - \frac{\mathrm{d}}{\mathrm{d}s}\left[\left(N + N_b + \frac{M + M_b}{\rho_o}\right)\psi_{o\eta\,b} + \left(N_b + \frac{M_b}{\rho_o}\right)\psi_{o\eta}\right] + f_{nb} = 0, \tag{33b}$$

which govern the post-buckling equilibrium. Boundary conditions of the buckled configuration can be prescribed for the following quantities

$$N_b|_{s(\pm\vartheta)} \qquad \text{or} \qquad u_{ob}|_{s(\pm\vartheta)}\ , \tag{34a}$$

$$\left[\frac{\mathrm{d}M_b}{\mathrm{d}s} - \left(N + N_b + \frac{M + M_b}{\rho_o}\right)\psi_{o\eta\,b} - \left(N_b + \frac{M_b}{\rho_o}\right)\psi_{o\eta}\right]\Bigg|_{s(\pm\vartheta)} \qquad \text{or} \qquad w_{ob}|_{s(\pm\vartheta)}\ , \tag{34b}$$

$$M_b|_{s(\pm\vartheta)} \qquad \text{or} \qquad \psi_{o\eta\,b}|_{s(\pm\vartheta)}\ . \tag{34c}$$

3.3 Differential Equations in Terms of Displacements

Observe that the structure of the equilibrium equation (33a) is very similar to that of $(11)_1$. The exception is the last term in (33a) when $f_{tb} = 0$, as it does not appear in the pre-buckling relation. However, that can be neglected since the product is quadratic in the increments. Therefore, repeating the line of thought leading to (14) and (15) for the increments it follows that the increment in the axial strain is constant

$$\frac{\mathrm{d}}{\mathrm{d}s}\left(A_e \varepsilon_{mb}\right) - \underbrace{\frac{1}{\rho_o}\left(A_e \varepsilon_m \psi_{o\eta b}\right)}_{\text{it can also be neglected}} = 0 \quad \Rightarrow \quad \frac{\mathrm{d}\varepsilon_{m\,b}}{\mathrm{d}s} \simeq \frac{\mathrm{d}\varepsilon_{o\xi\,b}}{\mathrm{d}s} = 0 \quad \rightarrow \quad \varepsilon_{m\,b} \simeq \varepsilon_{o\xi\,b} = \text{constant}\ . \tag{35}$$

We assume that $f_{nb} = 0$. If we (a) take into account that $\varepsilon_m^{(1)} = \varepsilon_{mb}^{(1)} = 0$; (b) substitute M_b form (29), and (c) utilize that

$$m\rho_o\varepsilon_{mb}\left(1 + \psi_{o\eta}^{(1)}\right) \simeq m\rho_o\varepsilon_{mb}\left[1 - \frac{1}{\rho_o}\left(w_o^{(2)} + w_o\right)\right] = m\rho_o\varepsilon_{mb} - m\varepsilon_{mb}\left(w_o^{(2)} + w_o\right)$$

(this relation can be set up in the same way as (16)) then, after some manipulations, (33b) yields

$$W_{ob}^{(4)} + (\chi^2 + 1)W_{ob}^{(2)} + \chi^2 W_{ob} = m\varepsilon_{mb}\left[1 - \left(W_o^{(2)} + W_o\right)\right]\ . \tag{36}$$

Here and in the sequel $W_{ob} = w_{ob}/\rho_o$ and $U_{ob} = u_{ob}/\rho_o$ are dimensionless displacement increments. Equation (36) is the post-buckling equilibrium equation in terms of W_{ob}.

Equation (39) published by Bradford et al. (2002) for stability investigations of shallow arches has the form

$$W_{ob}^{(4)} + (\chi^2 - 1)W_{ob}^{(2)} = m\varepsilon_{mb}\left(1 - W_o^{(2)}\right)\ . \tag{37}$$

3.4 General Solutions to the Post-buckling State

After substituting the pre-buckling solution (21) into the right side of equation (36) we get

$$W_{ob}^{(4)} + (1 + \chi^2)W_{ob}^{(2)} + \chi^2 W_{ob} = -m\varepsilon_{mb}\frac{1 - \chi^2}{\chi^2}\left(\frac{1}{1 - \chi^2} + A_3\cos\chi\varphi + A_4 H\sin\chi\varphi\right)\ . \tag{38}$$

Since $\varepsilon_{mb} = 0$ for antisymmetric buckling – see Bradford et al. (2002), Kiss and Szeidl (2014) –, differential equation (38) simplifies to

$$W_{ob}^{(4)} + (1 + \chi^2)W_{ob}^{(2)} + \chi^2 W_{ob} = 0\ . \tag{39}$$

The solution to it assumes the form

$$W_{ob} = E_1\cos\varphi + E_2\sin\varphi + E_3\sin\chi\varphi + E_4\cos\chi\varphi, \tag{40}$$

where E_i are undetermined integration constants.

Because $\varepsilon_{mb} =$ constant for symmetric buckling, we need the general solution of equation (38)

$$W_{ob}(\varphi) = C_1 \cos\varphi + C_2 \sin\varphi + C_3 \sin\chi\varphi + C_4 \cos\chi\varphi - \frac{m\varepsilon_{m\,b}}{2\chi^3}\left(\frac{2}{\chi} + A_3\varphi\sin\chi\varphi - A_4\varphi\cos\chi\varphi\right)\ ,\ \varphi\in[0,\vartheta] \tag{41}$$

in which C_i are undetermined integration constants. We remark that Figure 1 shows both the antisymmetric and the symmetric buckling shapes.

3.5 Solutions if $\varepsilon_{mb} = 0$

First, let us deal with the case when the length of the centerline does not change during buckling. Substitute solution (40) for the displacement increment W_{ob} if $\varepsilon_{mb} = 0$ into the boundary conditions presented in Table 2.

Table 2: Boundary conditions in terms of W_{ob} for fixed-fixed beams

Boundary conditions	
Left support	Right support
$W_{ob}\vert_{\varphi=-\vartheta} = 0$	$W_{ob}\vert_{\varphi=\vartheta} = 0$
$W_{ob}^{(1)}\Big\vert_{\varphi=-\vartheta} = 0$	$W_{ob}^{(1)}\Big\vert_{\varphi=\vartheta} = 0$

Nontrivial solution of the resulting system of equations exists if the characteristic determinant is zero

$$\mathfrak{D} = (\chi\sin\vartheta\cos\chi\vartheta - \cos\vartheta\sin\chi\vartheta)\,(\sin\vartheta\cos\chi\vartheta - \chi\cos\vartheta\sin\chi\vartheta) = 0\,. \tag{42}$$

Vanishing of the first factor yields the following equation

$$\chi\tan\vartheta = \tan\chi\vartheta\ . \tag{43}$$

The physically useful solution for $\chi\vartheta$ can be approximated with a good accuracy by the polynomial

$$\begin{aligned}\mathfrak{F} = \chi\vartheta = {} & 4.493\,419972 + 8.585\,048\,966\times10^{-3}\vartheta + 3.\,717\,588\,695\times10^{-2}\vartheta^2 + \\ & + 5.594\,338\,754\times10^{-2}\vartheta^3 - 3.056\,068\,806\times10^{-2}\vartheta^4 + 8.717\,756\,418\times10^{-3}\vartheta^5\,,\quad \vartheta\in[0.0,3.0]\ .\end{aligned} \tag{44}$$

It can be proven that an antisymmetric buckling shape belongs to this solution with $E_1 = E_4 = 0$ and $E_2 = -E_3\sin\chi\vartheta/\sin\vartheta$, therefore equation (40) yields

$$W_{ob} = E_3\left(\sin\chi\varphi - \frac{\sin\chi\vartheta}{\sin\vartheta}\sin\varphi\right)\ . \tag{45}$$

If $\sin\vartheta\cos\chi\vartheta - \chi\cos\vartheta\sin\chi\vartheta = 0$, then the smallest positive solution for $\chi\vartheta$ can be approximated with a good accuracy by two polynomials

$$\begin{aligned}\mathfrak{G} = \chi\vartheta = {} & 3.\,14159265 - 0.219\,240\,5286\vartheta + 1.558\,063\,614\vartheta^2 - 2.391\,954\,053\vartheta^3 + \\ & + 1.895\,751\,910\vartheta^4 - 0.441\,333\,7717\vartheta^5, && \text{if}\quad \vartheta\in[0,1.6] \\ \mathfrak{G} = \chi\vartheta = {} & -0.565\,27\vartheta^4 + 6.036\,1\vartheta^3 - 24.177\vartheta^2 + 43.533\vartheta - 23.981, && \text{if}\quad \vartheta\in[1.6,3.0]\ .\end{aligned} \tag{46}$$

It is worth mentioning that a symmetric buckling shape belongs to this solution with $E_2 = E_3 = 0$ and $E_4 = -E_1\sin\vartheta/(\chi\sin\chi\vartheta)$

$$W_{ob} = E_1\left(\cos\varphi - \frac{\sin\vartheta}{\chi\sin\chi\vartheta}\cos\chi\varphi\right)\ .$$

3.6 Solutions of Symmetric Buckling

To tackle the other type of buckling, i.e., when the strain does alter during the loss of stability, let us recall solution (41), which is now paired with the boundary conditions valid for a symmetric buckling shape – see Table 3.

Table 3: Boundary conditions in terms of W_{ob} for fixed-fixed beams

Boundary conditions	
Crown point	Right end
$W_{ob}^{(1)}(\varphi)\Big\vert_{\varphi=0} = 0$	$W_{ob}(\varphi)\vert_{\varphi=\vartheta} = 0$
$W_{ob}^{(3)}(\varphi)\Big\vert_{\varphi=0} = 0$	$W_{ob}^{(1)}(\varphi)\Big\vert_{\varphi=\vartheta} = 0$

The system of equations to be solved is

$$\begin{bmatrix} 0 & 1 & \chi & 0 \\ 0 & 1 & \chi^3 & 0 \\ \cos\vartheta & \sin\vartheta & \sin\chi\vartheta & \cos\chi\vartheta \\ \sin\vartheta & -\cos\vartheta & -\chi\cos\chi\vartheta & \chi\sin\chi\vartheta \end{bmatrix} \begin{bmatrix} C_1 \\ C_2 \\ C_3 \\ C_4 \end{bmatrix} = = m\varepsilon_{mb} \begin{bmatrix} -\frac{A_4}{2\chi^3} \\ -\frac{3A_4}{2\chi} \\ \frac{1}{2\chi^3}\left(\frac{2}{\chi} + A_3\vartheta\sin\chi\vartheta - A_4\vartheta\cos\chi\vartheta\right) \\ \frac{A_4}{2\chi^3}\left(\cos\chi\vartheta - \chi\vartheta\sin\chi\vartheta\right) - \frac{A_3}{2\chi^3}\left(\sin\chi\vartheta + \chi\vartheta\cos\chi\vartheta\right) \end{bmatrix} . \quad (47)$$

The solutions obtained can be given in the following forms

$$C_1 = \varepsilon_{mb}\left(\hat{C}_{11} + \hat{C}_{12}\frac{\mathcal{P}}{\vartheta}\right), \qquad C_4 = \varepsilon_{mb}\left(\hat{C}_{41} + \hat{C}_{42}\frac{\mathcal{P}}{\vartheta}\right), \quad (48a)$$

$$C_2 = \varepsilon_{mb}\hat{C}_{22}\frac{\mathcal{P}}{\vartheta}, \qquad C_3 = \varepsilon_{mb}\hat{C}_{32}\frac{\mathcal{P}}{\vartheta}, \quad (48b)$$

where

$$\hat{C}_{11} = m\frac{1}{2\chi^3\mathcal{D}}\left[2\sin\chi\vartheta + A_{31}\left(\cos\chi\vartheta\,\sin\chi\vartheta + \vartheta\chi\right)\right], \quad (49a)$$

$$\hat{C}_{12} = \frac{-m}{2\chi^3\left(1-\chi^2\right)\mathcal{D}}\left\{A_{32}\left(\chi^2-1\right)\left[\left(\cos\chi\vartheta\right)\sin\chi\vartheta + \vartheta\chi\right] + \right.$$
$$\left. + A_{42}\left[3\chi^2 - 2\chi^3\left(\sin\vartheta\right)\sin\chi\vartheta + \left(1-\chi^2\right)\cos^2\chi\vartheta - 2\chi^2\left(\cos\chi\vartheta\right)\cos\vartheta - 1\right]\right\}, \quad (49b)$$

$$\hat{C}_{22} = \frac{-mA_{42}}{\chi\left(1-\chi^2\right)}, \quad \hat{C}_{32} = \frac{m\left(3\chi^2-1\right)}{2\chi^4\left(1-\chi^2\right)}A_{42}, \quad (49c)$$

$$\hat{C}_{41} = m\frac{1}{2\chi^4\mathcal{D}}\left\{-2\sin\vartheta - A_{31}\left[\chi\left(\vartheta\sin\vartheta + \cos\vartheta\right)\sin\chi\vartheta + \vartheta\chi^2\cos\vartheta\cos\chi\vartheta\right]\right\}, \quad (49d)$$

and

$$\hat{C}_{42} = m\frac{1}{2\left(1-\chi^2\right)\chi^4\mathcal{D}}\Big\{A_{42}\left[\left[\left(1-\chi^2\right)\left(\vartheta\chi\cos\chi\vartheta - \sin\chi\vartheta\right) + 2\chi^2\left(\sin\chi\vartheta\right)\right]\sin\vartheta + \right.$$
$$+ \left(2\chi^3\cos\chi\vartheta - \vartheta\chi^2\left(1-\chi^2\right)\sin\chi\vartheta\right)\cos\vartheta - 2\chi^3\Big] +$$
$$\left. + A_{32}\left(\chi^2-1\right)\left[\chi\left(\vartheta\sin\vartheta + \cos\vartheta\right)\sin\chi\vartheta + \vartheta\chi^2\cos\vartheta\cos\chi\vartheta\right]\right\}. \quad (49e)$$

The solution (41) for W_{ob} and the angle of rotation $\psi_{o\eta\,b}$ can now be rewritten in the forms

$$W_{ob} = \varepsilon_{mb}\left[\left(\hat{C}_{01} + \hat{C}_{11}\cos\varphi + \hat{C}_{41}\cos\chi\varphi + \hat{C}_{51}\varphi\sin\chi\varphi\right) + \right.$$
$$\left. + \frac{\mathcal{P}}{\vartheta}\left(\hat{C}_{12}\cos\varphi + \hat{C}_{22}H\sin\varphi + \hat{C}_{32}H\sin\chi\varphi + \hat{C}_{42}\cos\chi\varphi + \hat{C}_{52}\varphi\sin\chi\varphi + \hat{C}_{62}H\varphi\cos\chi\varphi\right)\right], \quad (50)$$

$$-\psi_{o\eta\,b} \simeq W_{ob}^{(1)} = \varepsilon_{mb}\Big[K_{11}\sin\varphi + K_{41}\sin\chi\varphi + K_{51}\varphi\cos\chi\varphi +$$

$$+ \left(K_{12}\sin\varphi + K_{22}\cos\varphi + K_{32}\cos\chi\varphi + K_{42}\sin\chi\varphi + K_{52}\varphi\cos\chi\varphi + K_{62}\varphi\sin\chi\varphi\right)\frac{\mathcal{P}}{\vartheta}\Bigg] \,, \quad (51)$$

where

$$\begin{gathered} K_{11} = -\hat{C}_{11}\,, \qquad K_{41} = \hat{C}_{51} - \hat{C}_{41}\chi\,, \qquad K_{51} = \hat{C}_{51}\chi\,, \qquad K_{12} = -\hat{C}_{12}\,, \qquad K_{22} = \hat{C}_{22}H\,, \\ K_{32} = \hat{C}_{32}H\chi + \hat{C}_{62}H\,, \qquad K_{42} = \hat{C}_{52} - \hat{C}_{42}\chi\,, \qquad K_{52} = \chi\hat{C}_{52}\,, \qquad K_{62} = -\chi\hat{C}_{62}H \end{gathered} \quad (52)$$

are the new coefficients that have been introduced for the sake of brevity. If we neglect the effect of the tangential displacement on the angle of rotation then

$$\varepsilon_{mb} = \frac{1}{\vartheta}\int_0^{\vartheta}\left(U_{ob}^{(1)} + W_{ob} + W_o^{(1)}W_{ob}^{(1)}\right)\mathrm{d}\varphi \quad (53)$$

is the averaged strain increment. If we now substitute (50) and (51) into equation (53) then, after performing the integrations, we get

$$I_{13}\left(\frac{\mathcal{P}}{\vartheta}\right)^2 + \left[I_{02} + I_{12}\right]\frac{\mathcal{P}}{\vartheta} + \left[I_{01} + I_{11} - 1\right] = 0\,. \quad (54)$$

Here the coefficients (integrals) I_{01} and I_{02} are obtained from the second integral in (53) while the coefficients (integrals) I_{11}, I_{12} and I_{13} are from the third one. The first two integrals are presented in closed form in the Appendix – see equations (A.8a) and (A.8b). As regards integrals I_{11}, I_{12} and I_{13}, they are also given in Appendix – see equations (A.11), however, the closed forms are omitted. To compute the integrals we have used an IMSL subroutine with the name `DQDAG` – since its accuracy has proved to be extremely good.

4 Computational Results

4.1 Computational Steps

(a) The lower limit of antisymmetric buckling is obtained from the condition that the discriminant of (25) as a function of m should be real when the antisymmetric critical strain (44) is substituted into it. Consequently

$$\left[\left(I_{1w} + I_{1\psi}\right)^2 - 4I_{2\psi}(I_{ow} + I_{0\psi} - \varepsilon_m)\right]\Big|_{\mathfrak{F}=\chi\vartheta} \geq 0. \quad (55)$$

If the discriminant is positive, then equation

$$\frac{\mathcal{P}}{\vartheta} = \frac{-\left(I_{1w} + I_{1\psi}\right) \pm \sqrt{\left(I_{1w} + I_{1\psi}\right)^2 - 4I_{2\psi}(I_{0w} + I_{0\psi} - \varepsilon_m)}}{2I_{2\psi}} \quad (56)$$

gives the critical load. For a given m the discriminant as a function of ϑ has – according to the computational results – at least two roots for which it vanishes (then it becomes negative).

(b) Let $\chi\vartheta = \mathfrak{F}$. Then the nonlinear equations (25) and (54) with unknowns ε_m and $\mathcal{P}$ have no real roots.

(c) The lower limit of symmetric buckling, which is in general the limit below which there is no buckling at all, is obtained (i) by setting φ to 0 in equation (21), which now gives the vertical displacement at the crown point, (ii) substituting then the dimensionless force from (25) into the formula set up for the crown point displacements and finally (iii) taking the limit when $\chi\vartheta \to \mathfrak{G}$ keeping in mind that the displacement at the crown point should be real. The former condition yields the limit searched for.

(d) The displacement at the crown point as a function of the dimensionless force $\mathcal{P}$ (primary equilibrium path) is computed by using formulae (21) and (22).

4.2 Possible Buckling Modes

Similarly to the pinned-pinned beams, fixed-fixed ones can also buckle in a symmetric mode and in an antisymmetric mode, theoretically. However, the symmetric shape governs now the problem, which is exactly the contrary of what we have found in relation with pinned-pinned beams – see Kiss and Szeidl (2014). In this subsection

we again recall the results of Bradford et al. (2002), who found that their analytical results prove a reasonable approximation in accord with finite element calculations as long as $\vartheta \leq \pi/2$. Let us now introduce the modified slenderness ratio of the arch as

$$\lambda = \sqrt{m}\vartheta^2 = \frac{\sqrt{A_e \rho_o^2}}{\sqrt{I_e \eta}}\vartheta^2. \tag{57}$$

As regards the stability phenomenon, there are (a) two characteristic intervals if $m < 21\,148$, and (b) interestingly four if m is greater. A common thing is that for both cases there is no expected loss of stability when $\lambda(m)$ is sufficiently small. Then in case (a), there might only symmetric snap-through buckling occur for any greater λ-s. Considering the former case, i.e., the greater values of m and even the greater slenderness ratios, the interval of symmetric buckling is followed by a third range, where there appears the possibility of antisymmetric buckling along the symmetric one as well. At the same time, still the symmetric loss of stability is the dominant. It turns out that there is an upper limit for antisymmetric buckling beyond which the bifurcation point disappears. This separation is something Bradford et al. have not experienced. We have collected the typical stability intervals with their endpoints in Tables 4 and 5.

Table 4: Possible buckling modes of fixed-fixed beams with $m < 21\,148$

m		
$1\,000$	$10\,000$	
$\lambda < 11.61$	$\lambda < 11.15$	no buckling
$\lambda > 11.61$	$\lambda > 11.15$	limit point only

Table 5: Possible buckling modes of fixed-fixed beams with $m \geq 21\,148$

m			
$25\,000$	$100\,000$	$1\,000\,000$	
$\lambda < 11.12$	$\lambda < 11.06$	$\lambda < 11.02$	no buckling
$11.12 < \lambda < 53.77$	$11.06 < \lambda < 42.60$	$11.02 < \lambda < 39.4$	limit point only
$53.77 < \lambda < 86.33$	$42.60 < \lambda < 206.13$	$39.4 < \lambda < 672.15$	bifurcation point after limit point
$\lambda > 86.33$	$\lambda > 206.13$	$\lambda > 672.15$	limit point only

The approximative polynomials for the range boundaries are gathered hereinafter. For Bradford et al. there is no dependency on the parameter m. The lower limit of symmetric buckling is expressed via

$$\lambda(m) = \begin{cases} \dfrac{-1.74 \cdot 10^5}{m^2} + \dfrac{608}{m} + 11.186 - 4.8 \cdot 10^{-6}\, m + 5.2 \cdot 10^{-11}\, m^2 & \text{if } m \in [1\,000; 50\,000] \\ \dfrac{2530}{m} + 11.0363 - 8.7 \cdot 10^{-9}\, m & \text{if } m \in [50\,000; 1\,000\,000] \\ 11.02 & \text{in Bradford et al. (2002) p. 716.} \end{cases}$$

This is quite close to that of Bradford et al. but differ at most by 5.3%, when $m = 1\,000$.

As we find no upper limit for symmetric buckling we now move on to the lower limit of antisymmetric buckling that is

$$\lambda(m) = \begin{cases} \dfrac{2.4 \cdot 10^{44}}{m^{10}} - 0.085 \cdot m^{\frac{1}{2}} + 64.144 & \text{if } m \in [21\,148; 40\,000] \\ \dfrac{314\,000}{m} + 39 + 4.6 \cdot 10^{-6}\, m & \text{if } m \in [40\,000; 100\,000] \\ \dfrac{300\,000}{m} + 39.64 - 5.5 \cdot 10^{-7}\, m & \text{if } m \in [100\,000; 1\,000\,000] \\ 38.15 & \text{in Bradford et al. (2002) p. 716.} \end{cases}$$

While for Bradford et al. the outcome is valid for any m, we found the possibility of antisymmetric buckling only for $m \geq 21\,148$. The difference to the earlier model is $\approx 11\%$ if $m = 100\,000$, and is even more considerable with m decreasing. Compared to the results valid for pinned-pinned beams these figures are rather notable.

Finally, the upper limit of antisymmetric buckling is

$$\lambda(m) = \begin{cases} -90.3 - 2.27 \cdot 10^{-4}\, m - \dfrac{3.323 \cdot 10^{87}}{m^{20}} + 3.187\, m^{0.4} & \text{if} \quad m \in [21\,148; 10^5] \\ -10.1 - 2.628 \cdot 10^{-5} m + 0.617\, m^{0.51} & \text{if} \quad m \in [10^5; 10^6]. \end{cases}$$

Bradford et al. have not mentioned the possibility of this limit but in our model it exists. This, anyway, hugely depends on m. We may further remark that for fixed-fixed beams there is no intersection point of the symmetric and antisymmetric buckling curves.

4.3 Antisymmetric Loss of Stability

For our model the possibility of antisymmetric buckling is available only in a limited interval in $\lambda = \lambda(m)$. Figure 2 is obtained upon substituting the critical strain (44) into (25).

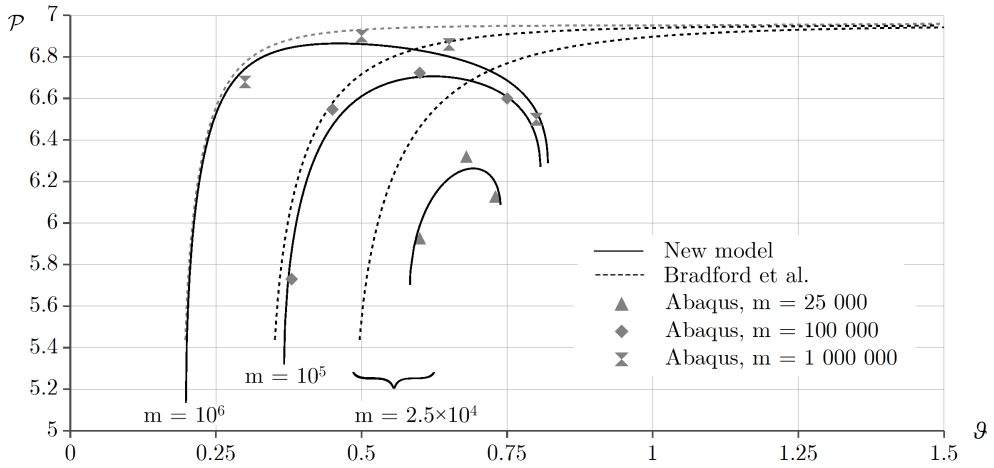

Figure 2: Antisymmetric buckling load against the semi-vertex angle

We have chosen three different magnitudes of m for the graphs to plot, and again show the results of Bradford et al. (2002) based on Figure 6 in the article cited. While the solution, which belongs to Bradford et al. tends to a certain loading value with ϑ increasing, our curves show a decrease after a while. For the two greatest values of m and for small central angles the outcome of both models seem to be quite close. However, due to the decrease even 10% distinction in the critical load is experienced if ϑ is greater. Choosing $m = 25\,000$, rather great differences (at least 11.2%) are experienced throughout.

Altogether, we may say that the new model always results in lower buckling loads. This is, however, not holding any remarkable meaning regarding the permissible load since – as we will present later on – the bifurcation point is always located beyond the limit point so symmetric buckling dominates. We also note that, as expected, fixed-fixed beams can bear heavier loads than pinned-pinned beams with the same material and geometry. We mention that finite element verifications were carried out for the buckling load of fixed-fixed beams using the commercial finite element software Abaqus 6.7. The cross-section considered was rectangular with $0.01\,[m]$ width and $0.005\,[m]$ height. The chosen Young's modulus was $2{\times}10^{11}\,[Pa]$. In Abaqus, we have used $B22$ elements and the Static,Riks step with geometrical nonlinearities. Initial geometric imperfections were introduced to the model via the first antisymmetric buckling mode of the beams, obtained from the linear perturbation, Buckle step. The magnitudes of the imperfections are collected in Table 6. Generally, there is quite a good correlation under these settings with our model.

Table 6: Comparison with FE calculations

m	ϑ	imperfection
25 000	0.6 / 0.68 / 0.73	$3.39 \cdot 10^{-3}$ / $3.24 \cdot 10^{-3}$ / $4.56 \cdot 10^{-3}$
100 000	0.38 / 0.45 / 0.6 / 0.75	$3.01 \cdot 10^{-3}$ / $3.58 \cdot 10^{-3}$ / $3.39 \cdot 10^{-3}$ / $6.6 \cdot 10^{-3}$
1 000 000	0.3 / 0.5 / 0.65 / 0.8	$2.43 \cdot 10^{-3}$ / $5.77 \cdot 10^{-3}$ / $1.12 \cdot 10^{-3}$ / $2.71 \cdot 10^{-2}$

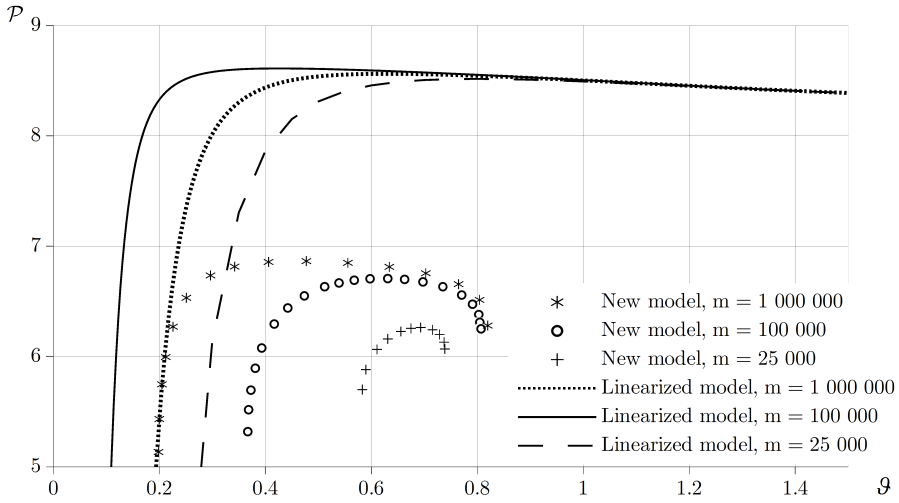

Figure 3: Antisymmetric buckling load - nonlinear versus linearized model

Drawing the linearized (the axial strain is considered to be linear) antisymmetric buckling curves, as can be seen in Figure 3, there are huge differences compared to the ones obtained within the frames of the nonlinear theory. The simplified model generally overestimates the critical load somewhere between 25% and 49% in $\mathcal{P}$. It is also clear that (a) the lower limits are as well different, and at the same time (b) there is no geometrical upper limit. If we recall the results of the linearized pinned-pinned model, where the differences were much less considerable, we can remark that the magnitude of the current figures are sort of surprising.

4.4 Symmetric Buckling

Dealing with the problem of symmetric buckling we have two equations to be solved simultaneously – equations (25) and (54) as not only the critical load but also the critical strain is unknown. The integrals in the second equation are to be taken from Appendix A.1.2 – see equations (A.1.2) and (A.11). The numerical results are compared to the model of Bradford et al. in Figure 4. Investigations by the authors cited show that their figures are more or less close to finite element calculations. Unfortunately, we can only make a comparison with the restriction that $\lambda \leq 100$ since Bradford et al. have not published results beyond this limit.

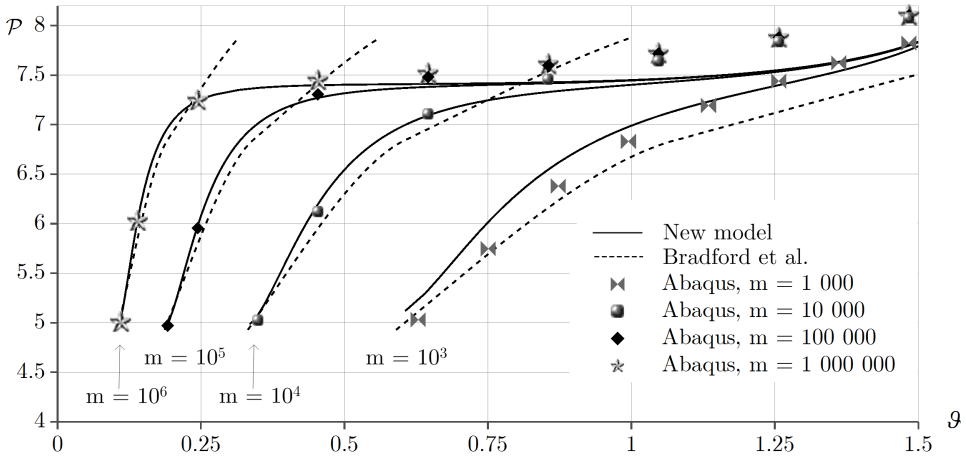

Figure 4: Symmetric buckling load against the semi-vertex angle

It is visible that if the angle is sufficiently great the results of the new model lead to the same critical load, independently of m. It is clear that at the beginning of the curves of both models generally yield very similar results. The lower m is the greater the differences are – for instance if $m = 1\,000$ and $\vartheta = 0.8$ it is up to 7%. When $m = 1\,000$ the characteristics of the corresponding curves are very similar, otherwise they show some distinction after a while. The greatest differences are up to 7.2% in the range in which we were able to carry out the comparison. It is also worthy of mentioning that for smaller central angles the model by Bradford et al. generally allows lower critical

loads, but this tendency changes with ϑ increasing. The exception is $m = 1\,000$, when the new model always yields greater permissible loads.

Some finite element verifications were carried out for the symmetric buckling load of fixed-fixed beams. The material, geometry and procedure are the same as mentioned in relation with antisymmetric buckling. However, this time initial imperfections are not used. Overall, there is quite a good correlation between the outcomes. The differences become greater, when the beams are nonshallow. It seems that the results of the Abaqus model also tend to a certain value for greater central angles. When $m = 1\,000$, the greatest difference is 5.1% at $\vartheta = 0.75$. When m is greater, the maximum difference between the models is 4.7% at $\vartheta = 1.48$. Therefore, the new model seems to be valid in the whole plotted interval.

The forthcoming relations fit well into the computational results presented in Figure 4

$$\mathcal{P}(m = 1\,000\,000, \vartheta) = \begin{cases} -0.037/\vartheta^2 + 8.09 - 3.75\,\vartheta^2 & \text{if} \quad \vartheta \in [0.11; 0.31] \\ -6.45 \cdot 10^{-4}/\vartheta^4 + 7.41 + 0.035\,\vartheta^6 & \text{if} \quad \vartheta \in [0.31; 1] \\ 7.245 + 0.195\vartheta + 7.7 \cdot 10^{-3}\vartheta^9 & \text{if} \quad \vartheta \in [1; 1.5] \end{cases} \tag{58a}$$

$$\mathcal{P}(m = 100\,000, \vartheta) = \begin{cases} -0.98/\vartheta + 10.04 - 41.56\,\vartheta^5 & \text{if} \quad \vartheta \in [0.19; 0.39] \\ -0.017/\vartheta^3 + 7.45 + 0.017\,\vartheta^8 & \text{if} \quad \vartheta \in [0.39; 1.5] \end{cases} \tag{58b}$$

$$\mathcal{P}(m = 10\,000, \vartheta) = \begin{cases} -1.87/\vartheta + 10.49 - 1.85\,\vartheta^3 & \text{if} \quad \vartheta \in [0.34; 0.72] \\ -0.436/\vartheta + 7.83 + 0.005\,\vartheta^{10} & \text{if} \quad \vartheta \in [0.72; 1.5] \end{cases} \tag{58c}$$

$$\mathcal{P}(m = 1\,000, \vartheta) = \begin{cases} -3.33/\vartheta + 10.54 - 0.22\,\vartheta^4 & \text{if} \quad \vartheta \in [0.606; 1.15] \\ -1.035/\vartheta^2 + 8.03 + 0.0017\,\vartheta^{12} & \text{if} \quad \vartheta \in [1.15; 1.5]. \end{cases} \tag{58d}$$

4.5 Load-crown Point Displacement Curves

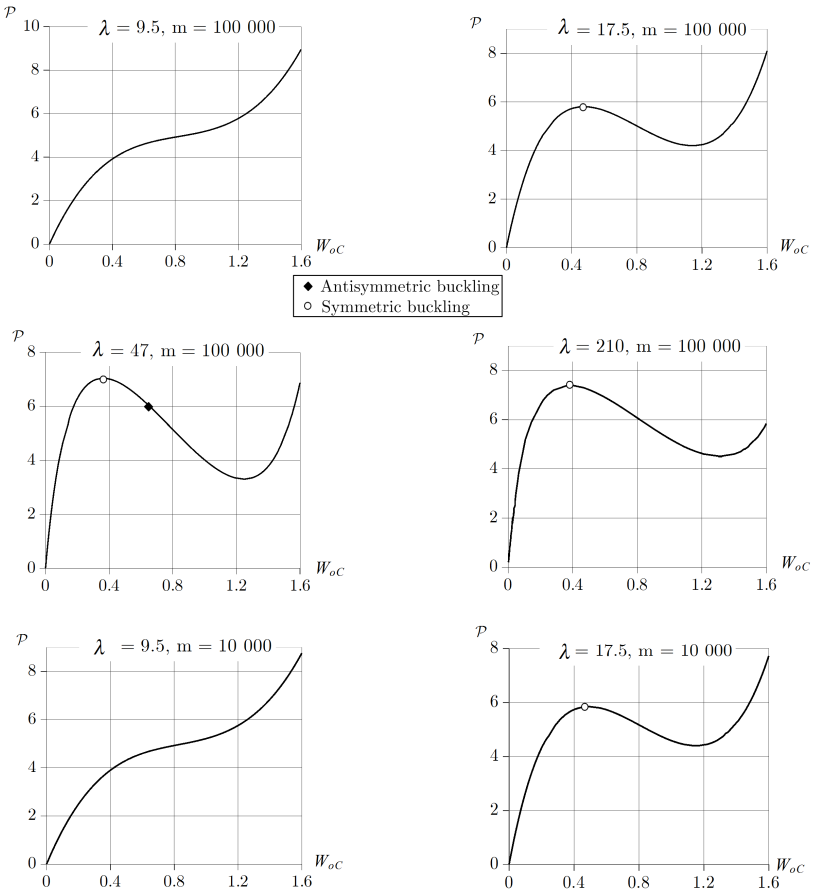

Figure 5: Dimensionless load versus the displacement at the crown point

Figure 5 presents the four possible primary paths (dimensionless load versus dimensionless crown point displacement curves) for beams with $m = 100\,000$ and the two characteristic modes when $m = 10\,000$ with

$$W_{oC} = \frac{-W_o|_{\varphi=0}}{1 - \cos\vartheta}. \tag{59}$$

W_{oC} is obtained by dividing the crown point displacement by the initial rise of the arch. Beams with small λ do not buckle. Increasing the slenderness ratio ($\lambda = 17.5$) results in the appearance of a limit point where $\partial\mathcal{P}/\partial W_{oC} = 0$. Thus, symmetric snap-through buckling takes place at the right loading level. This phenomenon is still independent of m. However, what follows next is only relevant when $m \geq 21\,148$. If $\lambda(m = 100\,000) = 47$ there is a bifurcation point located on the descending (unstable) branch of the load-deflection curve. Consequently, still the symmetric shape governs. If $\lambda(m = 100\,000) = 210$ there is no bifurcation point but only a limit point.

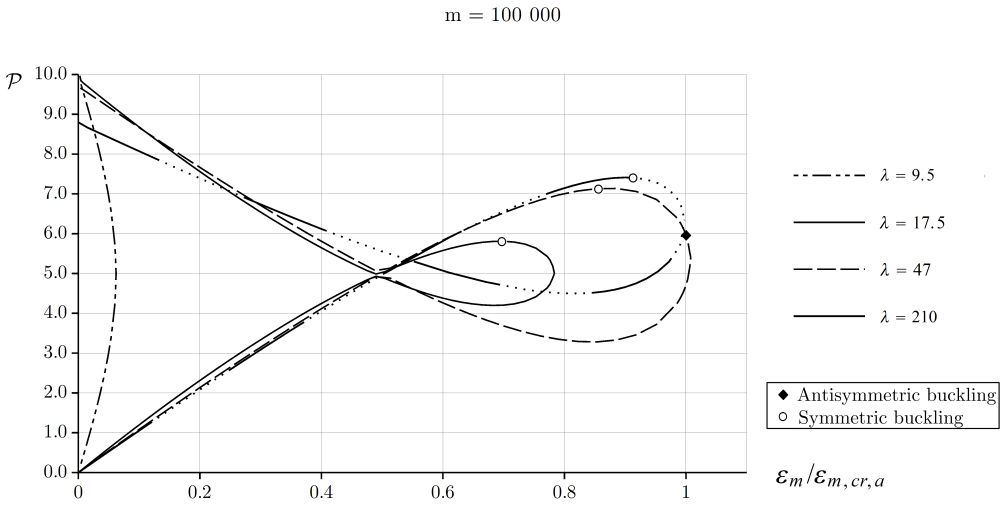

Figure 6: Dimensionless load-strain graphs, $m \geq 21\,148$

The typical dimensionless load $\mathcal{P}$ – strain/critical strain for antisymmetric buckling $\varepsilon_m/\varepsilon_{m\,cr\,a}$ graphs are shown separately in Figures 6 and 7 for $m \geq 21\,148$ and $m < 21\,148$. First let us fix m to 100 000. Choosing $\lambda = 9.5$ there are always two possible values of $\mathcal{P}$, and each one occurs once. If $\lambda = 17.5$ the two branches intersect each other at a certain point. On the branch, which starts from the origin we find a point where $\partial\mathcal{P}/\partial(\varepsilon_m/\varepsilon_{m\,cr\,a}) = 0$. This point relates to symmetric snap-through buckling. This type of buckling is the only possible option as $\varepsilon_m/\varepsilon_{m\,cr\,a}$ is always less than 1. By increasing the slenderness to 47, it can be seen that the critical antisymmetric strain is reached, i.e., antisymmetric buckling is also possible, but this point occurs after the limit point so still the symmetric shape is the dominant. Finally, when $\lambda = 210$ we find that the intersection point of the two branches are considerably further compared to the previous curves. The bifurcation point has vanished.

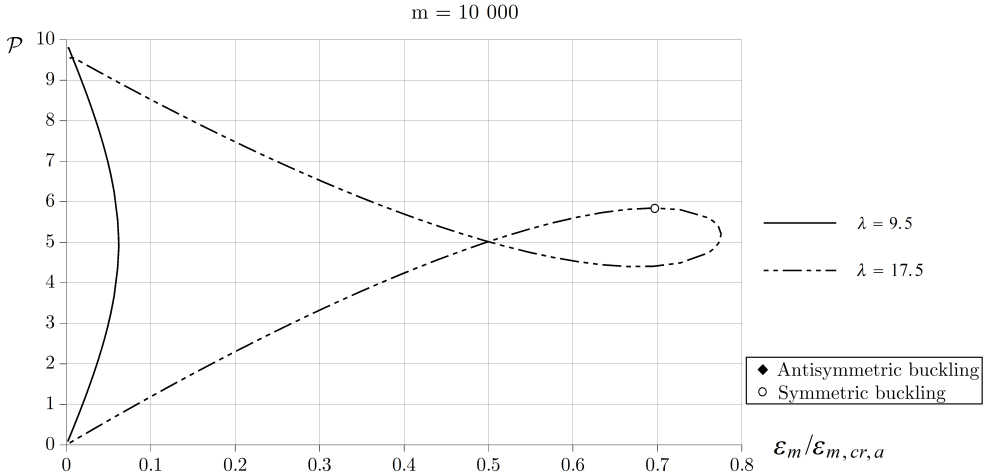

Figure 7: Dimensionless load-strain graphs, $m < 21\,148$

Decreasing m to 10 000 – see Figure 7 – there are two typical types of the $\mathcal{P} - \varepsilon_m/\varepsilon_{m\,cr\,a}$ curves, which coincide with the first two cases of the previous paragraph. Increasing the slenderness above 17.5 would never result in the

appearance of a bifurcation point.

We should remark that λ and m seem to have a considerable effect on where the upper branch commences on the vertical axis if ε_m is zero. The intersection point is also a function of these quantities. However, the lower branches always start from the origin.

5 Concluding Remarks

Under the assumption of cross-sectional inhomogeneity we have investigated the stability problem of fixed-fixed curved beams subjected to a central load. This paper is a continuation of the works Kiss and Szeidl (2014) and Kiss (2014), which study the same problem for pinned-pinned and rotationally restrained beams. The cross-sectional inhomogeneity is implied in the governing equations via the parameter χ, i.e., via the parameter m – see equations (5), (6), (7) and $(17)_2$. We would like to mention that equations (17) and (36) are more accurate than equations (18) and (37) solved by Bradford et al. (2002). We have neglected the effect of the tangential displacement on the angle of rotation – papers Pi et al. (2002) and Kiss and Szeidl (2014) also apply this assumption. Despite this neglect, with a regard to the more accurate problem formulation, we expected that the results for the critical load are more accurate than those published in Bradford et al. (2002).

Tables 4 and 5 present those intervals with their endpoints in which stability loss may occur. It has turned out that the possible buckling modes depend on the value of m: (a) if $m < 21\,148$ there is only limit point buckling (or no buckling), (b) if $m \geq 21\,148$ then, theoretically, both limit point buckling and bifurcation buckling might occur (or there is no buckling) depending on what value λ has.

As regards bifurcation buckling, it is worth emphasizing again that (a) this can take place in a limited interval in $\lambda = \lambda(m)$ – see Figure 2, (b) the critical force is less than that calculated by Bradford et al. (2002), (c) the bifurcation point is always located after the limit point. Therefore remarks (a) and (b) are of theoretical importance only, since the symmetric buckling dominates.

The results for symmetric buckling are presented in Figure 4. For smaller central angles the model by Bradford et al. generally allows lower critical loads, but this tendency changes with ϑ increasing. For $m = 1\,000$, however, the new model always yields greater permissible loads.

Acknowledgements by the first author: This research was supported by the European Union and the State of Hungary, co-financed by the European Social Fund in the framework of TÁMOP-4.2.4.A/ 2-11/1-2012-0001 'National Excellence Program'.

A.1 Detailed Manipulations

A.1.1 Calculation of the Pre-buckling Strain

Integral (24) is divided into two parts. The first part (the linear one) is as follows

$$\varepsilon_{o\xi} = \frac{1}{\vartheta}\int_0^{\vartheta} W_o \,\mathrm{d}\varphi = I_{ow} + I_{1w}\frac{\mathcal{P}}{\vartheta},$$

where

$$I_{ow} = \frac{\chi\left(\chi^2\vartheta - \vartheta + A_{11}\chi^2\sin\vartheta\right) - A_{31}\sin\chi\vartheta}{\vartheta\chi^3}\,, \tag{A.1a}$$

$$I_{1w} = \frac{A_{12}\chi^3\sin\vartheta + A_{22}\chi^3\left(1-\cos\vartheta\right) - A_{32}\sin\chi\vartheta + A_{42}\left(\cos\chi\vartheta - 1\right)}{\vartheta\chi^3}\,. \tag{A.1b}$$

By utilizing equations (23) for the nonlinear part integral, we can write

$$\frac{1}{\vartheta}\int_0^{\vartheta}\frac{1}{2}\psi_{o\eta}^2\left(\varphi\right)\mathrm{d}\varphi = I_{0\psi} + I_{1\psi}\frac{\mathcal{P}}{\vartheta} + I_{2\psi}\left(\frac{\mathcal{P}}{\vartheta}\right)^2\,. \tag{A.2}$$

Here

$$I_{0\psi} = \frac{1}{2\vartheta}\int_0^{\vartheta}\left(D_{11}\sin\varphi + D_{31}\sin\chi\varphi\right)^2\mathrm{d}\varphi = \frac{-1}{8\vartheta\chi\left(1-\chi^2\right)}\times$$

$$\times \left\{ D_{11}^2 \chi \left(\sin 2\vartheta - 2\vartheta \right) + \frac{8 D_{11} D_{31} \chi \left[\sin \chi\vartheta \, \cos\vartheta - \chi \sin\vartheta \, \cos \chi\vartheta \right]}{\left(1 - \chi^2 \right)} + D_{31}^2 \left(\sin 2\chi\vartheta - 2\vartheta\chi \right) \right\} . \quad \text{(A.3)}$$

To simplify the calculation, it is advisable to decompose $I_{1\psi}$

$$I_{1\psi} = \underbrace{\frac{1}{\vartheta} \int_0^{\vartheta} D_{11} \sin\varphi \left(D_{12} \sin\varphi + D_{22} \cos\varphi + D_{32} \sin\chi\varphi + D_{42} \cos\chi\varphi \right) \, \mathrm{d}\varphi +}_{I_{1\psi A}}$$

$$+ \underbrace{\frac{1}{\vartheta} \int_0^{\vartheta} D_{31} \sin\chi\varphi \left(D_{12} \sin\varphi + D_{22} \cos\varphi + D_{32} \sin\chi\varphi + D_{42} \cos\chi\varphi \right) \, \mathrm{d}\varphi}_{I_{1\psi B}} = I_{1\psi A} + I_{1\psi B}, \quad \text{(A.4)}$$

where

$$I_{1\psi A} = \frac{-D_{11}}{4\vartheta \left(1 - \chi^2 \right)} \left\{ D_{12} \left(1 - \chi^2 \right) \left(\sin 2\vartheta - 2\vartheta \right) + D_{22} \left(1 - \chi^2 \right) \left(\cos 2\vartheta - 1 \right) + \right.$$
$$\left. + 4 D_{32} \left[\sin\chi\vartheta \, \cos\vartheta - \chi \cos\chi\vartheta \, \sin\vartheta \right] + 4 D_{42} \left[\cos\vartheta \, \cos\chi\vartheta + \chi \sin\vartheta \, \sin\chi\vartheta - 1 \right] \right\} , \quad \text{(A.5a)}$$

and

$$I_{1\psi B} = \frac{D_{31}}{4\chi\vartheta \left(1 - \chi^2 \right)} \left\{ 4\chi D_{12} \left[\chi \sin\vartheta \, \cos\chi\vartheta - \sin\chi\vartheta \, \cos\vartheta \right] + \right.$$
$$\left. + 4\chi D_{22} \left[\sin\vartheta \, \sin\chi\vartheta + \chi \cos\vartheta \, \cos\chi\vartheta - \chi \right] + D_{32} \left(1 - \chi^2 \right) \left[2\vartheta\chi - \sin 2\chi\vartheta \right] + D_{42} \left(1 - \chi^2 \right) \left[1 - \cos 2\chi\vartheta \right] \right\} . \quad \text{(A.5b)}$$

Moving on now to the calculation of $I_{2\psi}$ in (A.2) it is again worth decomposing the factor in question but this time into four parts

$$\begin{aligned} I_{2\psi} = & \underbrace{\frac{1}{2\vartheta} \int_0^{\vartheta} \left(D_{12} \sin\varphi + D_{22} \cos\varphi + D_{32} \sin\chi\varphi + D_{42} \cos\chi\varphi \right) \, D_{12} \sin\varphi \mathrm{d}\varphi +}_{I_{2\psi A}} \\ & + \underbrace{\frac{1}{2\vartheta} \int_0^{\vartheta} \left(D_{12} \sin\varphi + D_{22} \cos\varphi + D_{32} \sin\chi\varphi + D_{42} \cos\chi\varphi \right) D_{22} \left(\cos\varphi \right) \, \mathrm{d}\varphi +}_{I_{2\psi B}} \\ & + \underbrace{\frac{1}{2\vartheta} \int_0^{\vartheta} \left(D_{12} \sin\varphi + D_{22} \cos\varphi + D_{32} \sin\chi\varphi + D_{42} \cos\chi\varphi \right) D_{32} \left(\sin\chi\varphi \right) \mathrm{d}\varphi +}_{I_{2\psi C}} \\ & + \underbrace{\frac{1}{2\vartheta} \int_0^{\vartheta} \left(D_{12} \sin\varphi + D_{22} \cos\varphi + D_{32} \sin\chi\varphi + D_{42} \cos\chi\varphi \right) D_{42} \left(\cos\chi\varphi \right) \, \mathrm{d}\varphi =}_{I_{2\psi D}} \\ & = I_{2\psi A} + I_{2\psi B} + I_{2\psi C} + I_{2\psi D} \, . \end{aligned} \quad \text{(A.6)}$$

The four terms in this sum are

$$I_{2\psi A} = \frac{1}{2\vartheta} \int_0^{\vartheta} \left(D_{12} \sin\varphi + D_{22} \cos\varphi + D_{32} \sin\chi\varphi + D_{42} \cos\chi\varphi \right) \, D_{12} \left(\sin\varphi \right) \mathrm{d}\varphi =$$
$$= \frac{D_{12}}{8\vartheta \left(1 - \chi^2 \right)} \left\{ D_{12} \left(1 - \chi^2 \right) \left[2\vartheta - \sin 2\vartheta \right] + D_{22} \left(1 - \chi^2 \right) \left[1 - \cos 2\vartheta \right] + \right.$$
$$\left. + 4 D_{32} \left(\chi \sin\vartheta \cos\chi\vartheta - \cos\vartheta \sin\chi\vartheta \right) + 4 D_{42} \left[1 - \cos\vartheta \cos\chi\vartheta - \chi \sin\vartheta \sin\chi\vartheta \right] \right\} , \quad \text{(A.7a)}$$

$$I_{2\psi B} = \frac{1}{2\vartheta} \int_0^{\vartheta} \left(D_{12} \sin\varphi + D_{22} \cos\varphi + D_{32} \sin\chi\varphi + D_{42} \cos\chi\varphi \right) D_{22} \left(\cos\varphi \right) \, \mathrm{d}\varphi =$$
$$= \frac{-D_{22}}{8\vartheta \left(\chi^2 - 1 \right)} \left\{ D_{12} \left(\chi^2 - 1 \right) \left(\cos 2\vartheta - 1 \right) - D_{22} \left(\chi^2 - 1 \right) \left(\sin 2\vartheta + 2\vartheta \right) + \right.$$
$$\left. + 4 D_{32} \left[\chi \left(\cos\chi\vartheta \right) \cos\vartheta + \left(\sin\chi\vartheta \right) \sin\vartheta - \chi \right] + 4 D_{42} \left[\left(\cos\chi\vartheta \right) \sin\vartheta - \chi \left(\sin\chi\vartheta \right) \cos\vartheta \right] \right\} , \quad \text{(A.7b)}$$

$$I_{2\psi C} = \frac{1}{2\vartheta} \int_0^{\vartheta} \left(D_{12} \sin\varphi + D_{22} \cos\varphi + D_{32} \sin\chi\varphi + D_{42} \cos\chi\varphi \right) D_{32} \left(\sin\chi\varphi \right) \mathrm{d}\varphi =$$
$$= \frac{D_{32}}{8\chi\vartheta \left(1 - \chi^2 \right)} \left\{ 4 D_{12} \chi \left[\chi \left(\cos\chi\vartheta \right) \sin\vartheta - \left(\sin\chi\vartheta \right) \cos\vartheta \right] + \right.$$

$$+4D_{22}\chi\left[(\sin\chi\vartheta)\sin\vartheta+\chi\left(\cos\chi\vartheta\right)\cos\vartheta-\chi\right]+D_{32}\left(1-\chi^2\right)\left[2\vartheta\chi-\sin 2\chi\vartheta\right]+D_{42}\left(1-\chi^2\right)\left[1-\cos 2\chi\vartheta\right]\Big\} \tag{A.7c}$$

and

$$I_{2\psi D}=\frac{1}{2\vartheta}\int_0^{\vartheta}\left(D_{12}\sin\varphi+D_{22}\cos\varphi+D_{32}\sin\chi\varphi+D_{42}\cos\chi\varphi\right)D_{42}\left(\cos\chi\varphi\right)\,\mathrm{d}\varphi=$$
$$=\frac{D_{42}}{8\vartheta\chi\left(\chi^2-1\right)}\left\{4D_{12}\chi\left[(\cos\chi\vartheta)\cos\vartheta+\chi\left(\sin\chi\vartheta\right)\sin\vartheta-1\right]+\right.$$
$$\left.+4D_{22}\chi\left[\chi\left(\sin\chi\vartheta\right)\cos\vartheta-\left(\cos\chi\vartheta\right)\sin\vartheta\right]+2D_{32}\left(\chi^2-1\right)\sin^2\chi\vartheta+2D_{42}\left(\chi^2-1\right)\left[\chi\vartheta+\left(\sin\chi\vartheta\right)\cos\chi\vartheta\right]\right\}. \tag{A.7d}$$

A.1.2 Calculation of the Averaged Strain Increment

Integrals I_{01} and I_{02} in (54) are given below in closed forms

$$I_{01}=\frac{1}{\vartheta}\int_0^{\vartheta}\left(\hat{C}_{01}+\hat{C}_{11}\cos\varphi+\hat{C}_{41}\cos\chi\varphi+\hat{C}_{51}\varphi\sin\chi\varphi\right)\mathrm{d}\varphi=$$
$$=\frac{1}{\chi^2\vartheta}\left[\chi^2\left(\hat{C}_{01}\vartheta+\hat{C}_{11}\sin\vartheta\right)+\hat{C}_{41}\chi\sin\chi\vartheta+\hat{C}_{51}\left(\sin\chi\vartheta-\chi\vartheta\cos\chi\vartheta\right)\right]\,, \tag{A.8a}$$

$$I_{02}=\frac{1}{\vartheta}\int_0^{\vartheta}\left(\hat{C}_{12}\cos\varphi+\hat{C}_{22}\sin\varphi+\hat{C}_{32}\sin\chi\varphi+\hat{C}_{42}\cos\chi\varphi+\hat{C}_{52}\varphi\sin\chi\varphi+\hat{C}_{62}\varphi\cos\chi\varphi\right)\mathrm{d}\varphi=$$
$$=\frac{1}{\chi^2\vartheta}\left[\chi^2\left(\hat{C}_{12}\sin\vartheta+\left(1-\cos\vartheta\right)\hat{C}_{22}\right)+\hat{C}_{52}\sin\chi\vartheta+\left(\cos\chi\vartheta-1\right)\hat{C}_{62}+\right.$$
$$\left.+\chi\left(\left(1-\cos\chi\vartheta\right)\hat{C}_{32}+\hat{C}_{42}\sin\chi\vartheta-\hat{C}_{52}\vartheta\cos\chi\vartheta+\hat{C}_{62}\vartheta\sin\chi\vartheta\right)\right]\,. \tag{A.8b}$$

Observe that I_{01} and I_{02} are the only integrals (constants), which appear in the part of the axial strain increment, which is obtained by neglecting the effect of the square of the rotation field. The corresponding expression, more precisely equation

$$I_{02}\frac{\mathcal{P}}{\vartheta}+I_{01}=1 \tag{A.9}$$

is linear in $\mathcal{P}$. As for the second integral in (53) let us recall formulae (23), (51) and (52). Consequently, we get

$$\frac{1}{\vartheta\varepsilon_{mb}}\int_0^{\vartheta}W_o^{(1)}W_{ob}^{(1)}\mathrm{d}\varphi=I_{13}\left(\frac{\mathcal{P}}{\vartheta}\right)^2+I_{12}\frac{\mathcal{P}}{\vartheta}+I_{11} \tag{A.10}$$

in which

$$I_{11}=-\frac{1}{\vartheta}\int_0^{\vartheta}\left(K_{11}\sin\varphi+K_{41}\sin\chi\varphi+K_{51}\,\varphi\cos\chi\varphi\right)\left(D_{11}\sin\varphi+D_{31}\sin\chi\varphi\right)\mathrm{d}\varphi\,, \tag{A.11a}$$

$$I_{12}=-\frac{1}{\vartheta}\int_0^{\vartheta}\left(D_{11}\sin\varphi+D_{31}\sin\chi\varphi\right)\times$$
$$\times\left(K_{12}\sin\varphi+K_{22}\cos\varphi+K_{32}\cos\chi\varphi+K_{42}\sin\chi\varphi+K_{52}\varphi\cos\chi\varphi+K_{62}\varphi\sin\chi\varphi\right)\mathrm{d}\varphi-$$
$$-\frac{1}{\vartheta}\int_0^{\vartheta}\left(K_{11}\sin\varphi+K_{41}\sin\chi\varphi+K_{51}\,\varphi\cos\chi\varphi\right)\left(D_{12}\sin\varphi+D_{22}\cos\varphi+D_{32}\sin\chi\varphi+D_{42}\cos\chi\varphi\right)\mathrm{d}\varphi\,, \tag{A.11b}$$

$$I_{13}=-\frac{1}{\vartheta}\int_0^{\vartheta}\left(D_{12}\sin\varphi+D_{22}\cos\varphi+D_{32}\sin\chi\varphi+D_{42}\cos\chi\varphi\right)\times$$
$$\times\left(K_{12}\sin\varphi+K_{22}\cos\varphi+K_{32}\cos\chi\varphi+K_{42}\sin\chi\varphi+K_{52}\varphi\cos\chi\varphi+K_{62}\varphi\sin\chi\varphi\right)\mathrm{d}\varphi\,. \tag{A.11c}$$

We would like to emphasize that the above integrals can all be given in closed forms. We omit them from being presented here as these are very complex. Mathematical softwares like Maple 16 or Scientific Work Place 5.5 can cope with these constants easily. Our aim was just to demonstrate the possibility of such solution.

References

Baksa, A.; Ecsedi, I.: A note on the pure bending of nonhomogenous prismatic bars. *International Journal of Mechanical Engineering Education*, 37, 2, (2009), 118–129.

Bateni, M.; Eslami, M. R.: Non-linear in-plane stability analysis of FGM circular shallow arches under central concentrated force. *International Journal of Non-Linear Mechanics*, 60, (2014), 58–69.

Bradford, M. A.; Uy, B.; Pi, Y. L.: In-plane elastic stability of arches under a central concentrated load. *Journal of Engineering Mechanics*, 128, 7, (2002), 710–719.

Chen, Y.; Feng, J.: Elastic stability of shallow pin-ended parabolic arches subjected to step loads. *Journal of Central South University of Technology*, 17, (2010), 156–162.

Chen, Y.; Feng, J.; Zhang, Y.: A necessary condition for stability of kinematically indeterminate pin-jointed structures with symmetry. *Mechanics Research Communications*, 60, (2014), 64–73.

Ecsedi, I.; Dluhi, K.: A linear model for the static and dynamic analysis of non-homogeneous curved beams. *Applied Mathematical Modelling*, 29, 12, (2005), 1211–1231.

Kiss, L.: A possible model for heterogenous curved beams. *Multidiszciplináris Tudományok*, 2, 1, (2012), 61–76 (in Hungarian).

Kiss, L.: In-plane buckling of rotationally restrained heterogeneous shallow arches subjected to a concentrated force at the crown point. *Journal of Computational and Applied Mechanics*, 9, 2, (2014), 171–199.

Kiss, L.; Szeidl, G.: In-plane stability of pinned-pinned heterogeneous curved beams under a concentrated radial load at the crown point. *Technische Mechanik*, (in press).

Pi, Y. L.; Bradford, M. A.: Dynamic buckling of shallow pin ended arches under a sudden central concentrated load. *Journal of Sound and Vibration*, 317, (2008), 898–917.

Pi, Y.-L.; Bradford, M. A.: Non-linear buckling and postbuckling analysis of arches with unequal rotational end restraints under a central concentrated load. *International Journal of Solids and Structures*, 49, (2012), 3762–3773.

Pi, Y. L.; Bradford, M. A.; Tin-Loi, F.: Non-linear in-plane buckling of rotationally restrained shallow arches under a central concentrated load. *International Journal of Non-Linear Mechanics*, 43, (2008), 1–17.

Pi, Y. L.; Bradford, M. A.; Uy, B.: In-plane stability of arches. *International Journal of Solids and Structures*, 39, (2002), 105–125.

Silveira, R. A. M.; Nogueira, C. L.; Goncalves, P. B.: A numerical approach for equilibrium and stability analysis of slender arches and rings under contact constraints. *International Journal of Solids and Structures*, 50, (2013), 147–159.

Address: Institute of Applied Mechanics, University of Miskolc, 3515 Miskolc-Egyetemváros, Hungary
email: mechkiss@uni-miskolc.hu, gyorgy.szeidl@uni-miskolc.hu